Catalysis Today 164 (2011) 395–398

Contents lists available at ScienceDirect

Catalysis Today

journal homepage: www.elsevier.com/locate/cattod

Photocatalytic decomposition of methylene blue over yttrium ion doped Ti-SBA-15 catalysts

Won Young Jung[a], Gun Dae Lee[b], Seong Soo Park[b], Kwon Taek Lim[c], Seong-Soo Hong[a,*]

[a] Department of Chemical Engineering, Pukyong National University, 100 Yongdang-dong, Nam-ku, Busan 608-739, Republic of Korea
[b] Industrial Chemistry, Pukyong National University, 100 Yongdang-dong, Nam-ku, Busan 608-739, Republic of Korea
[c] Image System Engineering, Pukyong National University, 100 Yongdang-dong, Nam-ku, Busan 608-739, Republic of Korea

ARTICLE INFO

Article history:
Received 21 June 2010
Received in revised form
19 November 2010
Accepted 21 November 2010
Available online 18 December 2010

Keywords:
Yttrium doped Ti-SBA-15
Hydrothermal method
Photocatalytic decomposition of methylene blue

ABSTRACT

Ti-SBA-15 catalysts doped with yttrium ion were synthesized using conventional hydrothermal method and they were characterized by XRD, FT-IR, NH_3-TPD and PL. We also examined the activity of these materials on the photocatalytic decomposition of methylene blue. With increasing the doping amount of yttrium ion, the surface area and pore volume of Y/Ti-SBA-15 materials were increased. 1 mole% Y/Ti-SBA-15 catalysts showed the highest photocatalytic activity on the decomposition of methylene blue but the catalysts doped with more than 2 mole% Y/Ti-SBA-15 showed lower activity compared to pure Ti-SBA-15 catalyst.

1. Introduction

Heterogeneous photocatalysis, a semiconductor mediated catalytic process, is shown to be a promising technology to degrade a wide range of organic pollutants [1–4]. Among various metal oxide semiconductors, titania, especially anatase phase, has been proven to be one of the most efficient photocatalysts due to its chemical stability, relatively low price, non-toxicity and optical and electronic properties. To maximize photocatalytic activity of TiO_2, particles should be small enough to offer a high specific surface area. Unfortunately, for applications in aqueous phase such as a small particle size means high filtration costs to remove the catalyst once the reaction is finished. These problems have motivated the development of supported photocatalysts in which TiO_2 has been immobilized on diverse materials [5].

The incorporation of transition-metal ions into the frameworks of the molecular sieves is a general method for introducing catalytic sites into mesoporous material. Especially, the introduction of Ti-containing mesoporous materials has added a new dimension to the application of mesoporous materials in oxidation catalysis [6]. These efforts have resulted in a successful synthesis of hydrothermally stable SBA-15 silica molecular sieve with uniform hexagonal channels ranging from 50 to 300 Å. In the previous study, Ti-substituted SBA-15 materials were prepared by microwave-hydrothermal method and they showed a good photocatalytic activity on the degradation of orange II [7].

In order to slow down the electron–hole pairs enhance interfacial efficiency, several attempts have been proposed, including transition metals doping, coupled semiconductor system, noble metals deposition. Especially, doping with lanthanide ions with 4f electron configurations could enhance the photocatalytic activity of TiO_2 [8–11].

However, no effort using the yttrium ion doped titanium dioxide for the photocatalytic degradation of organic dyes was shown. Therefore, in this study, yttrium ion doped Ti-containing SBA-15 samples were prepared by hydrothermal method. The physical properties of prepared Y/Ti-containing SBA-15 samples were investigated and we also examined the activity of them for the photocatalytic decomposition of methylene blue.

2. Experimental

Ti-substituted SBA-15 materials (Si/Ti = 30) were synthesized by hydrothermal method using tetraethyl orthosilicate (TEOS) and titanium tetraisopropoxide (TTIP) as the sources of Si and Ti, respectively. In addition, appropriate amount of yttrium nitrate was added as a source of yttrium oxide. 4.06 g of Pluronic P123 triblock copolymer surfactant ($EO_{20}PO_{70}EO_{20}$, M_{av} = 5800) and 0.68 g of PEG (polyethyleneglycol)) were dissolved in 160 mL of distilled

* Corresponding author at: Department of Chemical Engineering, Pukyong National University, 100 Yongdang-dong, Nam-ku, Busan 608-739, Republic of Korea.
E-mail address: sshong@pknu.ac.kr (S.-S. Hong).

0920-5861/$ – see front matter © 2010 Elsevier B.V. All rights reserved.
doi:10.1016/j.cattod.2010.11.047

water and 10 mL of 2 M HCl was added drop wise to the solution as a catalyst. The mixed solution was transferred to a 250 mL Teflon container held in a stainless-steel vessel. After the vessel was tightly sealed, it was heated at 80 °C for 48 h. After hydrothermal treatment, the synthesized materials were washed in distilled water and were dried at 105 °C for 12 h, and were then calcined at 500 °C for 6 h.

The major phase of the obtained particles was analyzed by X-ray diffraction (Rigaku D/MAXIIC) using Cu Kα radiation. The chemical structure of the prepared particles was examined using the Fourier transform infrared spectrophotometer (FT-IR, Bruker, IFS-88) in the 400∼4000 cm^{-1} frequency range. The BET surface area of the prepared particles was determined by nitrogen physisorption data at 77 K using a Micromeritics ASAP 2400 and pore volume and pore size distribution were determined by the BJH (Barrett–Joyner–Halenda) method. UV–vis diffuse reflectance spectroscopy (DRS) was performed on Varian Cary 100 with PTFE (polytetrafluoroethylene) as standard. The photoluminescence (PL) spectra of the samples were recorded with a Fluorescence spectrophotometer F-4500. Temperature-programmed desorption (TPD) of ammonia experiments were carried out using 100 mg catalysts under a gas flow (100 mL/min) of NH_3 (2000 ppm) diluted with helium. Mass spectrometer (HPR 20) was used to monitor the ammonia desorption amount.

A biannular quartz glass reactor with a lamp immersed in the inner part of the reactor was used for all the photocatalytic experiments. The samples were immediately centrifuged and the quantitative determination of methylene blue was performed by a UV–vis spectrophotometer (Shimazu UV-240). The reactor was filled with 100 mL of an aqueous dispersion in which the concentration of photocatalyst and of methylene blue were 0.1 g/L and 100 mg/L, respectively and magnetically stirred to maintain uniform concentration and temperature.

3. Results and discussion

Fig. 1 shows XRD patterns of Ti-SBA-15 and Y/Ti-SBA-15 materials. Calcined siliceous Ti-SBA-15 and Y/Ti-SBA-15 samples with varying yttrium ion doping displayed well-resolved pattern with a sharp peak at about 1.0° that matched well with the reported pattern [9]. With an increase of doping amount of yttrium ions, the XRD peaks show a well-resolved pattern. This result indicates that Y/Ti-SBA-15 materials maintain the mesoporous structure regardless of the doping of yttrium ion.

Table 1 shows the textural properties of Ti-SBA-15 and Y/Ti-SBA-15 materials. It is clear that the surface area and pore volume of Y/Ti-SBA-15 materials are increased in the yttrium ions doping on the silica matrix. The increase of the surface area in the doping of yttrium ions on Ti-SBA-15 material is caused by an inhibitory effect to the sintering of nano-sized titania [10].

Fig. 2 shows the adsorption–desorption isotherms of Ti-SBA-15 and Y/Ti-SBA-15 materials. As it can be observed, Ti-SBA-15 and Y/Ti-SBA-15 materials exhibit the type IV nitrogen isotherm with desorption hysteresis loops types H2, which is characteristic of mesoporous materials [11]. The size of hysteresis increases in the doping of yttrium ions on Ti-SBA-15 material and also increases with increasing the yttrium ions doping amount. The big hysteresis is attributed to the existence of pore cavities larger than the openings (throats), leading to ink-bottle pores [12].

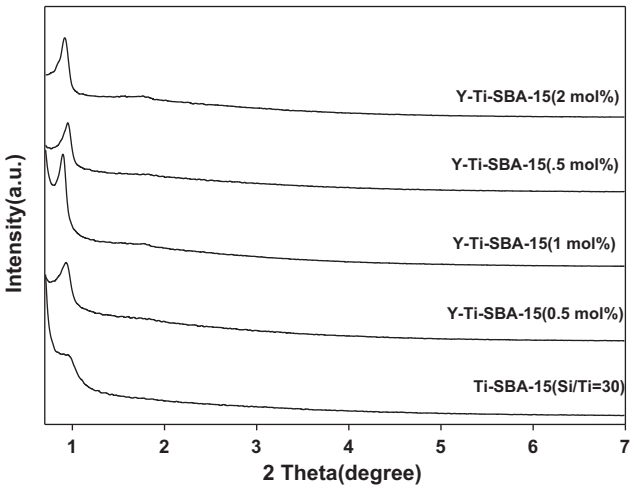

Fig. 1. X-ray diffraction patterns of Ti-SBA-15 and various Y/Ti-SBA-15 catalysts.

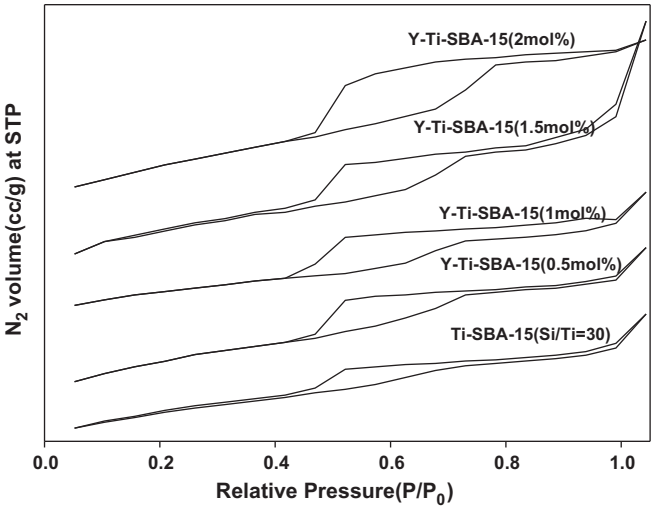

Fig. 2. N_2 adsorption/desorption isotherm of Ti-SBA-15 and various Y/Ti-SBA-15 catalysts.

Fig. 3 shows the IR spectra of Ti-SBA-15 and Y/Ti-SBA-15 materials. For all samples, the IR absorption at about 960 cm^{-1} commonly accepted the characteristic vibration of Ti–O–Si bond regardless of the doping of yttrium ion. This result indicates that systematic increase in intensity of IR absorption is generally taken as a proof of Ti incorporating into the framework of zeolite [13]. The wave numbers of 460, 800 and 1100 cm^{-1} in Fig. 3 indicate the band for Si–O–Si bond. In addition, the band at 1640 cm^{-1} was ascribed to the bending vibration absorption of free water.

Table 1
Textural properties of Y/Ti-SBA-15 catalysts and their photocatalytic activity on the decomposition of methylene blue.

Catalyst	Surface area (m^2/g)	Pore volume (cm^3/g)	Pore size (nm)	Catalytic activity k' ($\times 10^{-2}$ min^{-1})
Ti-SBA-15 (Si/Ti = 30)	870	9.5	4.4	1.5
Y/Ti-SBA-15 (0.5 mole%)	1013	11.0	4.3	2.9
Y/Ti-SBA-15 (1.0 mole%)	982	12.6	4.3	3.4
Y/Ti-SBA-15 (1.5 mole%)	1005	12.8	4.0	1.4
Y/Ti-SBA-15 (2.0 mole%)	1002	10.0	3.6	0.6
P-25	–	–	–	1.9

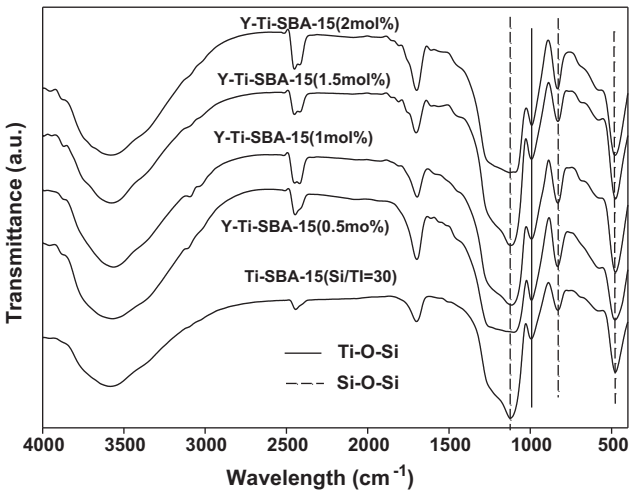

Fig. 3. FT-IR spectra of Ti-SBA-15 and various Y/Ti-SBA-15 catalysts.

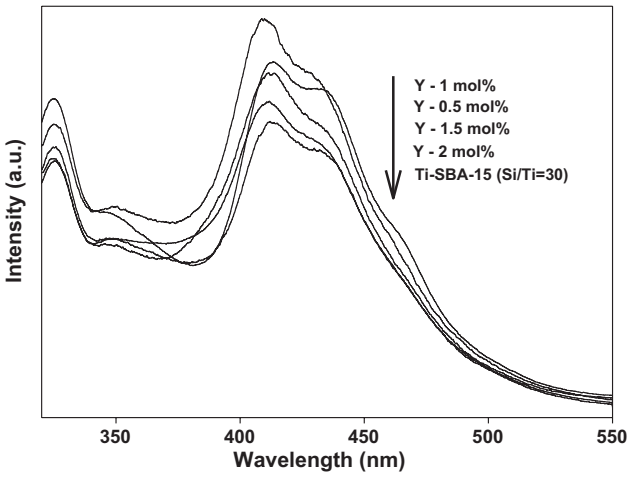

Fig. 5. PL spectra of Ti-SBA-15 and various La/Ti-SBA-15 catalysts.

Fig. 4 shows the UV–visible diffuse reflectance spectra (DRS) of yttrium doped TiO_2 particles in the range of 200–500 nm. It is well known that DRS can be used to investigate the optical absorption properties of photocatalysts. There is no absorption in the visible region (>400 nm) regardless of doping of yttrium ions to TiO_2 particles and the broad bands at 220 nm appeared at the Y/Ti-SBA-15 samples, indicating framework incorporation of titanium into SBA-15. In addition, the optical absorption in the UV region is shown to have the same order of photocatalytic activity.

Fig. 5 shows the PL spectra of Y/Ti-SBA-15 samples with various amounts of yttrium ion. It is shown that the undoped and doped Ti-SBA-15 samples can give obvious excitonic PL signals with similar shape, demonstrating that yttrium dopant does not give rise to new PL phenomena. In addition, the excitonic PL signal shows the highest intensity in the case of 1.0 mole% Y/Ti-SBA-15 sample.

It is well known that titania particles exhibit the strong and wide PL signals at the range from 400 to 500 nm with the excited wavelength of 300 nm. For the La-Ti-SBA-15 samples, two obvious PL peaks appeared at about 410 and 430 nm, respectively. It is thought that the former peak is mainly due to band edge free exactions and the latter is due to the binding exactions. The stronger the excitonic PL signal, the higher the content of surface oxygen vacancy and defect. In addition, during the process of the photocatalytic reaction, oxygen vacancy and defect can become the centers to capture photoinduced electrons so that the recombination of photoinduced electrons and holes can be inhibited. Moreover, oxygen vacancies can promote the adsorption of oxygen and then the strong interaction between the photoinduced electrons bound by oxygen vacancies and adsorbed oxygen can be formed. This result indicates that the binding for the photoinduced electrons of oxygen vacancies can make the capture for photoinduced electrons of adsorbed oxygen and oxygen radical group was produced at the same time. Therefore, oxygen vacancy and defect are in favor of photocatalytic reactions in that oxygen is active to promote the oxidation of organic substances. This suggests that the stronger the PL intensity, the larger the amount of oxygen vacancy and defect, the higher the photocatalytic activity. As shown in Fig. 5, the photocatalytic activity on the decomposition of methylene blue shows the same order with the intensity of PL peaks of Y/Ti-SBA-15 samples.

Fig. 6 shows photocatalytic decomposition of methylene blue over Y/Ti-SBA-15 catalysts under UV illumination.

It is well known that photocatalytic oxidation of organic pollutants follows Langmuir–Hinshelwood kinetics [14,15], with the rate being proportional to the coverage θ:

$$r = -\frac{dc}{dt} = k\theta = k\frac{KC}{1+KC} \quad (1)$$

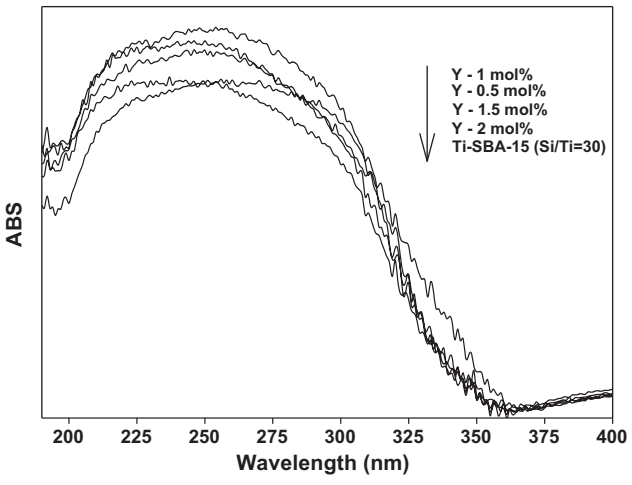

Fig. 4. UV–visible diffuse reflectance of Ti-SBA-15 and various Y/Ti-SBA-15 catalysts.

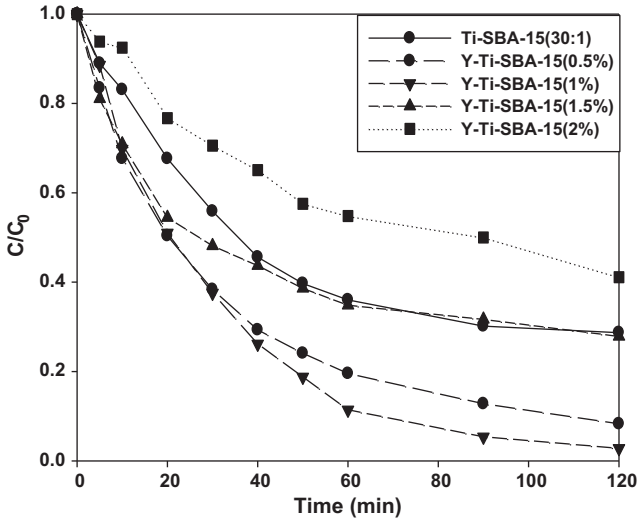

Fig. 6. Photocatalytic activity of Ti-SBA-15 and various Y/Ti-SBA-15 catalysts.

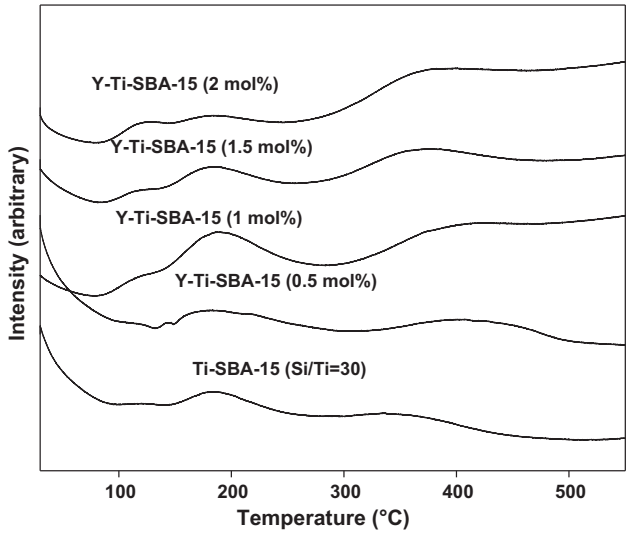

Fig. 7. Ammonia TPD spectra of Ti-SBA-15 and various Y/Ti-SBA-15 catalysts.

where k is the true rate constant which is dependent upon various parameters such as mass of catalyst, the flux of efficient, the coverage in oxygen, etc., K the adsorption coefficient of the reactant, and C the reactant concentration. When C is very small, the product KC is negligible with respect to unity so that Eq. (1) describes a first-order kinetics. Setting the Eq. (1) at the initial conditions of the photocatalytic procedure, $t = 0$, the concentration transforms to $C = C_0$, which gives Eq. (2).

$$-\ln\left(\frac{C}{C_0}\right) = k_{app}t \tag{2}$$

where k_{app} is the apparent first-order reaction constant.

The photocatalytic activity on the decomposition of methylene blue over Y/Ti-SBA-15 catalysts is shown in Table 1 and Fig. 5. When blank test in the absence of photocatalyst was carried out, methylene blue was decomposed to about 10% after 3 h reaction by photolysis reaction. The 1 mole% Y^{3+}-doped Ti-SBA-15 catalyst shows the highest activity on the photocatalytic decomposition of methylene blue but the activity decreases doped more than 2 mole% of yttrium ion compared to Ti-SBA-15 catalyst. As shown in Fig. 3, the photocatalytic activity for the decomposition of methylene blue is proportional to the intensity of the PL peaks of the yttrium doped Ti-SBA-15 materials. It was reported that doping with lanthanide ions with 4f electron configurations could significantly enhance the photocatalytic activity of TiO_2 [16]. It was also reported that an optimum doping of rare earth ions in TiO_2 particles for the most efficient separation of photoinduced electron–hole pairs [17]. As mentioned above, the stronger the PL intensity, the larger the amount of oxygen vacancies and defects, and the higher the photocatalytic activity.

Fig. 7 shows the temperature programmed desorption (TPD) of ammonia for Y/Ti-SBA-15 catalysts. The ammonia desorption peak is shown at 190 °C and 1 mole% Y/Ti-SBA-15 catalyst shows the highest intensity of the peak. In addition, the order of desorption peak intensity is proportional to the photocatalytic activity. It is well known that methylene blue used in this study is classified by basic pigment. Therefore, it is assigned that the stronger ammonia desorption peak intensity, the large amount of acidic site, the higher photocatalytic activity owing to much adsorption of reactants.

4. Conclusion

Ti-SBA-15 catalysts doped with yttrium ion were synthesized using conventional hydrothermal method and they were characterized by XRD, FT-IR, NH_3-TPD and PL. We also examined the activity of these materials on the photocatalytic decomposition of methylene blue. Y/Ti-SBA-15 materials maintain the mesoporous structure regardless of the doping of yttrium ion. With increasing the doping amount of lanthanide ion, the surface area and pore volume of Y/Ti-SBA-15 materials. 1 mole% Y/Ti-SBA-15 catalyst showed the highest photocatalytic activity on the decomposition of methylene blue and it showed the strongest PL peak intensity and ammonia desorption peak intensity.

Acknowledgements

This research was supported by Basic Science Research Program through the National Research Foundation of Korea (NRF) funded by the Ministry of Education, Science and Technology (No. 2010-0016900) and Brain Busan 21 Project in 2010.

References

[1] R.S.G. Ferreira, P.G.P. Oliveira, F.B. Noronha, Appl. Catal. B 29 (2001) 275.
[2] G.J. Hutchings, C.S. Heneghan, I.D. Hudson, S.H. Taylor, Nature 384 (1996) 341.
[3] W. Nam, K. Woo, G. Han, J. Ind. Eng. Chem. 15 (2009) 348.
[4] W.C. Oh, F.J. Zhang, M.L. Chen, Y.M. Lee, W.B. Ko, J. Ind. Eng. Chem. 15 (2009) 190.
[5] M.T. Bore, H.N. Pham, E.E. Switzer, T.L. Ward, A. Fukuoka, A.K. Datye, J. Phys. Chem. B 109 (2005) 2873.
[6] B. Notari, Adv. Catal. 41 (1996) 253.
[7] W.Y. Jung, S.H. Baek, G.D. Lee, S.S. Park, E.D. Jeong, H.G. Kim, S.S. Hong, React. Kinet. Catal. Lett. 91 (2007) 233.
[8] V. Iliev, D. Tomova, Appl. Catal. B 63 (2006) 266.
[9] G. Li, X.S. Zhao, Ind. Eng. Chem. Res. 45 (2006) 3569.
[10] M. Saif, M.S.A. Abdel-Mottaleb, Inorg. Chim. Acta 360 (2007) 2863.
[11] S.J. Gregg, K.S.W. Sing, Adsorption, Surface Area and Porosity, Academic Press, London, 1982.
[12] T. Lopez, F. Rojas, R. Alexander-Katz, F. Galindo, A. Balankin, A. Buljan, J. Solid State Chem. 177 (2004) 1873.
[13] M.D. Alba, Z. Luan, J. Klinowski, J. Phys. Chem. 100 (1996) 2178.
[14] S.S. Hong, M.S. Lee, J.H. Kim, B.H. Ahn, K.T. Lim, G.D. Lee, J. Ind. Eng. Chem. 8 (2002) 150.
[15] C.S. Turchi, D.F. Ollis, J. Catal. 122 (1995) 178.
[16] X. Yan, J. He, Appl. Catal. B 55 (2005) 243.
[17] A.W. Xu, Y. Gao, H.Q. Liu, J. Catal. 207 (2002) 151.